4-(9-Anthryl)aniline. 2. Two Weakly-Coupled Electronic States and their Torsional Potentials Evaluated from the Laser-Induced Fluorescence Spectra in a Supersonic Jet

Seonkyung Lee and Okitsugu Kajimoto*

Department of Chemistry, Graduate School of Science, Kyoto University, Kitashirakawa-Oiwakecho, Sakyo-ku, Kyoto 606-01, Japan

Received: January 24, 1997; In Final Form: May 15, 1997[⊗]

Laser-induced fluorescence excitation spectra of 4-(9-anthryl)aniline (AA) have been observed in a free jet. A detailed analysis of the spectra reveals the presence of a new low-lying charge-transfer (CT) state. Taking account of a coupling of this CT state with the locally excited (LE) state, we reproduced the spectra and evaluated the torsional potentials of the ground, the LE, and the CT states. In an isolated AA molecule, the CT state is nonperpendicular and charge separation is incomplete. The presence of the NH_2 substituent is responsible for the low-lying CT state while the flexibility in torsional motion yields the nonperpendicular CT state. These findings are the key to understanding the so-called multistate CT in 4-(9-anthryl)-dimethylaniline and its homologues.

Introduction

The torsional vibration of biaryl molecules about a single bond plays important roles in many aspects of molecular structure and dynamics.[1−5] The torsional potential function reflects the operation of chemical forces such as conjugation and repulsive nonbonding interactions between two aryl groups. When biaryl molecules possess both electron-donating and electron-accepting parts within a molecule, they often form an intramolecular charge-transfer (ICT) state. The torsional motion has been considered to have a close relation with the efficiency of the ICT state formation.[6,7]

In 1968, Lippert[8] first found an abnormally red-shifted emission on photoexcitation of 9,9′-bianthryl (BA) in polar solvents, in contrast to the ordinary fluorescence from the locally excited (LE) state. This abnormal fluorescence was later assigned to a twisted intramolecular charge-transfer (TICT) state, whose donor and acceptor parts are perpendicular to each other. Later, Mataga et al.[9] found similar behavior for 4-(9-anthryl)-dimethylaniline (ADMA). However, the dynamics of the TICT formation in the latter compound is very complex and cannot be analyzed using the ordinary two-state model, which assumes only two relevant states (the LE and the charge-transfer (CT) states) and well reproduces the behavior of BA.[10,11] Such a contrasting behavior between these anthracene derivatives may be attributable to the difference in the torsional potential in the excited state, since the torsional motion is the key reaction coordinate for the TICT state formation. On the other hand, Zachariasse discussed the electronic states of several TICT molecules and claimed that in the case of 4-(*N*,*N*-dimethylamino)benzonitrile (DMABN) the interaction between the LE state and the closely-lying CT state is more important than the torsional motion as the factor controlling the CT state formation.[12] Thus, the information about the low-lying electronic states of ADMA must also be important to clarify the strange behavior in the CT state formation dynamics.

Wortmann et al.[13] recently succeeded in determining the torsional potential of BA in solution and found that the equilibrium angle is about 60°, slightly smaller than that in the gas phase,[14] and becomes further smaller in polar solvents. For ADMA, however, the determination of the torsional potentials is quite difficult because of its spectral congestion and the lack of information of the gas phase potentials. We have attempted to determine the equilibrium torsional angle of ADMA in a free jet, but the laser-induced fluorescence (LIF) spectra were congested too much to deduce the torsional potential.[15]

In the present study, therefore, we synthesized 4-(9-anthryl)-aniline (AA), which is a simple homologue of ADMA with a reduced number of internal rotors, and obtained less congested spectra suitable for the detailed analysis of the torsional potential. In the preceding paper in this issue we have shown that the new compound, AA, gives an intramolecular charge-transfer state just like ADMA in polar solvents and reported several features of the CT state. In the present paper, we report the LIF excitation spectra and the high-resolution LIF spectra of AA taken in a free jet. The presence of a new low-lying electronic state is proposed, and the torsional potentials for the three electronic states are determined. The new electronic state and the torsional potentials turn out to be the key in solving the outstanding questions about the peculiar behavior of ADMA in the CT state formation.

Experimental Section

The LIF excitation spectra were obtained with a pulsed-jet apparatus. The sample was placed inside a pulsed valve and heated to about 150 °C to increase the concentration of AA in a jet. Helium carrier gas was expanded through a 0.8 mm diameter nozzle into a vacuum chamber at a repetition rate of 5 Hz. The background pressure of the chamber was kept below 10^{-4} Torr during the experiments. The laser beam was provided by a dye laser (Lambda Physik, LPD 3002E) pumped by an excimer laser (Lambda Physik, LPX 105*i*). The laser beam crossed the supersonic jet 20 mm downstream from the nozzle in most cases. In order to change the cooling conditions, the nozzle−laser distance and the stagnation pressure were changed. The intensity of the laser beam was monitored by a photodiode. The fluorescence was collected through a lens and fed into a photomultiplier (Hamamatsu R928). Both signals were processed with boxcare integrators (SRS 250) and stored in a microcomputer. The observed LIF signal was normalized by the laser intensity. The rotational band contours were recorded using an intracavitiy etalon with a resolution of about 0.04 cm^{-1}.

[⊗] Abstract published in *Advance ACS Abstracts,* July 1, 1997.

S1089-5639(97)00331-9 CCC: $14.00

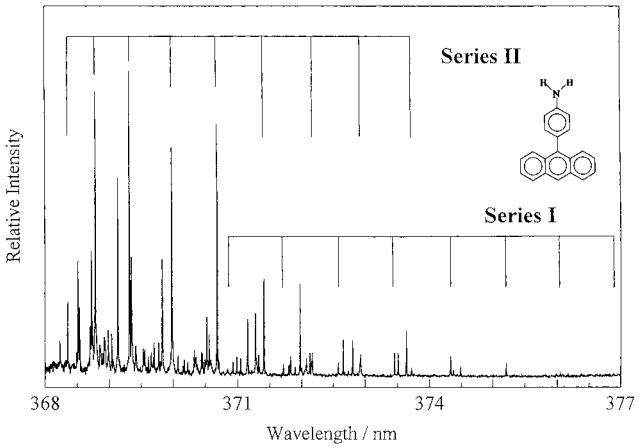

Figure 1. LIF excitation spectrum of AA, composed of two kinds of progressions. The torsional progression is bracketed in each series.

TABLE 1: Fundamental Frequencies of the Low-Frequency Vibrational Modes in the Electronically Excited State

mode	vibrational frequency, cm^{-1}	torsional spacing in each mode, cm^{-1}
	Series I	
A	63	63
B	116	60
C	184	62
D	301	60
	Series II	
	231	56 (average)

Fluorescence lifetimes were determined by the time-correlated single-photon counting method using a mode-locked Ti:sapphire laser (Spectra-Physics, Tsunami model 3950) which was pumped by a continuous wave argon ion laser (Spectra-Physics, Beamlock 2060). The laser pulse was focused into a $LiIO_3$ crystal to generate second-harmonic radiation. The UV light crossed the jet at a distance of 20 mm downstream from the nozzle. The fluorescence was collected using a two-lens system, and detected with a Hamamatsu R2809-02u microchannel plate (MCP) photomultiplier tube. The output of the MCP was fed through a high-speed preamplifier and a constant fraction discriminator (Tennelec TC455) and into a time-to-amplitude converter. The full width at half-maximum of the instrument response function for the detection system was about 30 ps.

Results

1. General Features of the LIF Spectra of AA. The LIF excitation spectrum of 4-(9-anthryl)aniline (AA) between 368 and 377 nm is shown in Figure 1. The general features of this spectrum are similar to those in the ADMA spectrum[15] except that the peaks observed are sharp and are separated from each other. The LIF spectrum consists of the 0−0 transition groups and the vibronic transition groups associated with the 12_0^1 (a fundamental frequency of 386 cm^{-1}), 12_0^2 (769 cm^{-1}) and 6_0^1 (1389 cm^{-1}) bands of the anthracene vibrational modes.[16] As already reported in the previous paper,[17] this spectrum is analyzed as being composed of two different series. From hole-burning spectroscopy, it was confirmed that all the peaks in this region correspond to the transitions from the common and unique level of the ground state.

The two series of progressions show quite different features in their intensities and distributions. Series I appears in the longer wavelength region with weak intensity and an equal peak spacing of 63 cm^{-1}. The peak intensity is the largest around the center of the progression. Series II is observed in the shorter wavelength region with strong intensity and an energy level spacing decreasing with increasing transition energy. The spectral intensity of the series II peaks is generally more than 10 times stronger than that of the series I peaks. The observed spectroscopic transitions and fundamental frequencies, in the range 368−377 nm, are summarized in Table 1. The fundamental frequencies given in Table 1 may include some uncertainty, because we estimated the frequencies by assuming that the peak at the longest wavelength in each progression belongs to the same torsional quantum number (the peak at the longest wavelength is not necessarily the origin of the torsional progression).

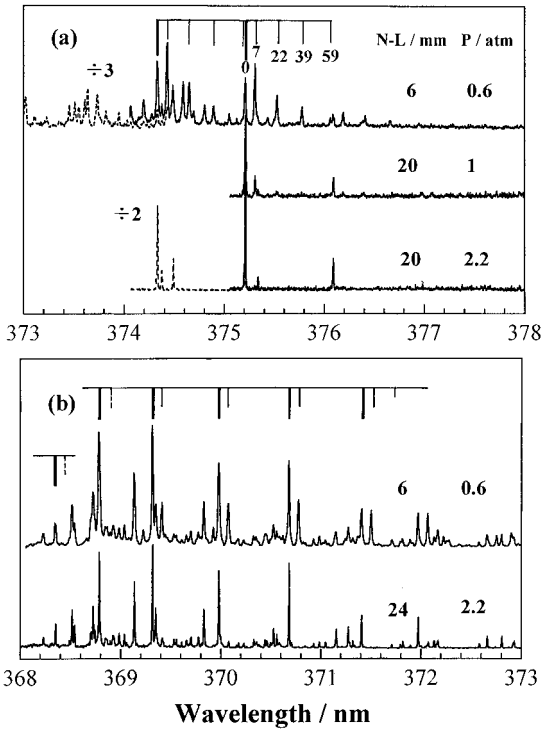

Figure 2. LIF excitation spectra with changing cooling conditions, showing the growth of the hot band peaks: (a) the hot band peaks observed in series I progression and their frequencies and (b) the hot band peaks for the series II progression. The intensity of the first hot band (7 cm^{-1} red-shifted) relative to the parent peak changes with the transition energy.

The vibrational structure of series II is similar to that reported for the derivatives of 9-phenylanthracene (9-PA)[18] in their spacing and intensity distributions. This fact strongly indicates that the series II progression is ascribable to the torsional vibration around the anthryl−aniline bond in the first excited allowed electronic state. On the other hand, series I is a characteristic progression induced by the presence of the NH_2 group and is missing in other 9-PA derivatives. In addition, the low-frequency combination bands with torsional progressions (denoted as B, C, and D) are observed in series I. In contrast, the series II progression does not have such low-frequency torsional progressions, in accordance with the observed trend in 9-PA. These combination bands in series I may be related to the vibrations in the aniline moiety which has several vibrational modes with the frequencies of 100−300 cm^{-1}.[19]

2. Hot Band LIF Spectra. 2.1. Assignment of the Hot Bands. The LIF excitation spectra in Figure 2a demonstrate the effects of changing the cooling conditions. At higher temperatures, one can observe hot bands appearing 7, 22, 39, and 59 cm^{-1} red-shifted from the corresponding parent peaks. Although weak, the intensities of these hot bands clearly increase

with decreasing stagnation pressure, i.e., with increasing temperature. These hot bands can be interpreted either as a v''-progression or as a Δv sequence between the ground and the excited states. The latter possibility is, however, excluded when one considers the energy spacing of the upper torsional vibration and the jet temperatures. Thus, all the hot bands were assigned to the v''-progression, and hence the hot vibrational levels in the ground electronic state were directly obtained from the frequencies of the hot bands relative to the parent peak.

Using the torsional energy levels obtained above, the torsional potential curve of the ground state was calculated by the procedure given in the Discussions section 2. This potential curve was utilized for the simulation of the rotational band contours and also for the calculation of the Franck−Condon factors. Generally speaking, the dispersed fluorescence spectra are suitable to obtain information on the ground state vibrational levels. However, the dispersed fluorescence spectra of AA are much too congested to make the straightforward assignment of the spectral features.

2.2. Dependence of the Hot Band Characters on the Series. The observed hot bands show noticeable differences between the two series. First, in series I, all the hot bands at 7, 22, 39, and 59 cm^{-1} are observed for every parent peak, as illustrated in Figure 2a, even in the higher torsional levels. On the other hand, in series II, the number of the hot bands observed depends on the vibronic levels, as demonstrated in Figure 2b: all the hot bands are detected in the lower transition energy region, only the peak red-shifted by 7 cm^{-1} is detectable in the middle region, and no hot bands are observed in the higher energy region of the progression. Second, the intensity ratio between the 7 cm^{-1} hot band and its parent peak is different in the two series. The ratio is almost the same (at a specific temperature) in all the parent peaks of series I whereas in series II the intensity ratio decreases with increasing transition energy.

The above two features stem from the same reason, that is, the change of the Franck−Condon factor with increasing ground state torsional level. In series I, the Franck−Condon overlap between the ground and the excited states becomes favorable for higher torsional levels, while in series II it becomes unfavorable. This trend is important in relation to the nature of the electronic state which generates each series of the progression. The detailed discussion will be given later.

3. Rotational Band Contours. In order to determine the structure of AA in the upper vibronic level, we measured the rotational band contours for several single-vibronic transitions. Figure 3 shows the rotational band contours obtained for both the series I and II transitions. Generally, for the peaks in the 0−0 band region, a sharp Q branch and comparatively narrow P and R branches are observed, which is a distinctive feature of an A-type transition. The three spectra in Figure 3 suggest that the rotational contours are very similar between the series I and II progressions. In addition, the relative intensities among the P, Q, and R branches do not change significantly with increasing transition energy.

The above observation leads us to the following conclusions. First, the electronic transitions to both electronic states (series I and II) are A-type, indicating that the electronic state which induces the transitions in both series has a transition moment directing parallel to the anthryl−aniline bond. Next, the similarity in the shape of the rotational band contours indicates that the rotational constants of the upper torsional level do not change significantly within the energy range observed.

Rotational band contours were simulated with the torsional angle (and hence the rotational constants) as fitting parameters. The results are shown in Figure 4 along with the equilibrium

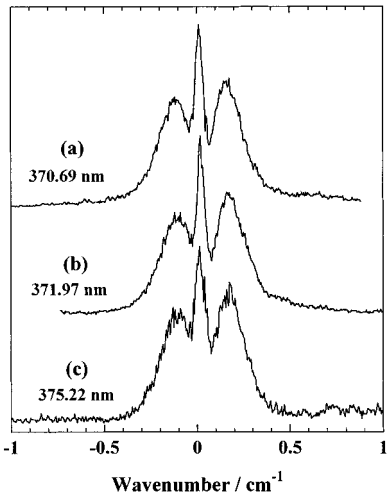

Figure 3. Rotational band contours in selected single vibronic peaks. The peak in (a) belongs to the series II progression while those of (b) and (c) belong to the series I progression.

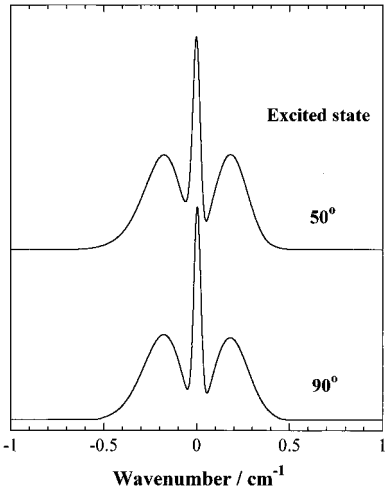

Figure 4. Simulated rotational band contours with two typical equilibrium torsional angles of the excited state. The equilibrium angle of the ground state is taken to be 90°.

torsional angles of the upper and lower states. The rotational constants of the ground and the excited states were calculated by varying the length of the anthryl−aniline bond and the equilibrium torsional angle. The rotational constants of the ground state were estimated by assuming the equilibrium angle of 90°. Varying the rotational constants of the upper state affected primarily the relative intensities among the P and R branches and hence the band symmetry. The best fit was obtained when the rotational constants of the upper state were evaluated using the equilibrium angle of 50°, together with a 0.02 Å decrease of the anthryl−aniline bond length upon excitation.

4. Lifetimes of Each Series. If the observed two series of progressions were ascribed to simple vibrational combinations on the same electronic state, the lifetime must be very similar between the two series. In order to check this possibility, fluorescence decays were measured for selected peaks. For series I, the peaks of the B mode progression were selected because the peak intensities of the A mode progression are insufficient for the precise measurement. The fluorescence decay curves for several selective transitions in each series are plotted in Figure 5, and the evaluated lifetimes are listed in Table 2. The observed decay curves can be fitted by using a single-exponential function, except the peaks around 373 nm. The peaks in series I give lifetimes of about 10 ns whereas those in

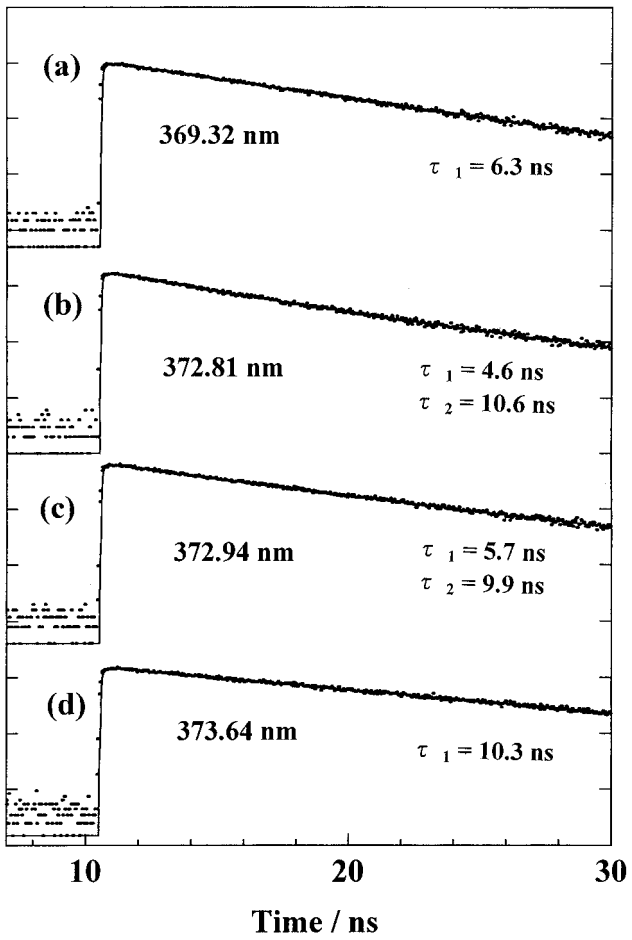

Figure 5. Fluorescence decay curves for selected peaks. The traces (a) and (d) are for the peaks of the series II and I progressions, respectively. Those of (b) and (c) are for the peaks around 373 nm, and their decay curves cannot be fitted with a single-exponential function.

TABLE 2: Fluorescence Lifetimes for the Selected Peaks of AA

excitation energy, cm^{-1}	lifetime, ns
26 764	10.3
26 814[a]	5.7, 9.9
26 823[a]	4.6, 10.6
26 884	9.3
26 924	6.3
26 977	8.6
27 028	5.8
27 077	6.3
27 116	5.9

[a] The decay curves are represented by double-exponential functions.

series II have lifetimes of about 6 ns. Although the difference is not large, it is certain that the upper electronic state for each series decays with each intrinsic lifetime. This fact strongly supports the presence of two different electronic states, each of them yielding the different progression.

Peculiar behavior in the decay curves was observed for the peaks between 372 and 373 nm. The decay curves were only well represented by double-exponential functions with lifetimes which are slightly different from those of series I and II. Two typical decay curves are shown in Figure 5b,c. A high-resolution LIF measurement of these peaks revealed that each of them consists of two or three peaks closely overlapping with each other. The double-exponential decay is, therefore, interpreted as a result of simultaneous excitation of two independent species, each belonging to the different series. The appearance of such closely-lying peaks with different origins suggests that the two electronic states most probably cross with each other around this energy region.

Discussions

In the present section, we first summarize the experimental findings described in the preceding section and then try to determine the torsional potentials based on the observed energy levels and transition intensities. In the course of deducing the torsional potentials, we again find that the assumption of the two electronically excited states is essential for the reproduction of the observed LIF spectra. The torsional potentials of the zero-order electronic states are determined first, and then the coupling between the two electronic states is introduced. The intensities of the observed LIF spectra of both series are well reproduced by the simulation. In the subsequent section, we briefly discuss the nature of the new electronic state in terms of molecular orbitals obtained from simple semiempirical calculations (CNDO/S). Finally, the implication of the new electronic state to the charge-transfer dynamics of AA and ADMA is discussed.

1. The Two Excited Electronic States of AA. The peaks belonging to the different progressions show quite different behavior in many respects: their lifetimes, the features in the LIF spectra, and the feasibility in observing the hot bands. We suppose that these two transitions with quite different natures correspond to the transitions to two different electronic states and hereafter try to characterize the origin of these electronic states. In the following, we will consider a rough picture of the electronic states and the torsional potentials, as inferred from the observations. Three electronic states, one ground and two excited states, are involved in the present studies. For the ground electronic state, the discussion will be postponed to a later section where quantitative calculations of transition intensities will be given on the basis of the Franck−Condon factors between the ground and the excited states. Briefly, the ground state potential should be very flat around 90° in order to reproduce the observed characteristics of the hot bands.

1.1. Series II Progression. Now, let us consider in detail the upper electronic state giving the series II progression. As pointed out in the previous section, the spectroscopic features of the series II progression are quite similar to those of 9-PA: the decreasing level spacing and the increasing peak intensity with increasing transition energy and also the lack of low-frequency combination bands accompanied by the torsional progression. According to the analysis by Werst et al.,[18] 9-PA has a ground state potential whose minimum is located at 90°, and the shape at the bottom is rather flat. The excited state potential is reported to have double minima at 60° with a barrier height of 250 cm^{-1}. It is, therefore, natural to expect a similar situation for AA: the ground electronic state having a minimum at 90° and the excited state with a double-minimum potential. From the spectral range of the progression, we can estimate the barrier of the double-minimum potential to be more than 400 cm^{-1}. The result of the contour analysis suggests the excited state equilibrium angle to be 50° and the transition is A-type. Since 9-PA is a rather simple aromatic compound, this transition can be attributed mostly to the $\pi-\pi^*$ transition localized in the anthracene moiety, that is, the transition to the LE state, which is an A-type transition.

1.2. Series I Progression. On the other hand, series I differs from series II in many respects: much smaller intensities than series II, equal spacing of 63 cm^{-1}, and longer lifetimes. On the basis of rotational contour analysis, however, the transition

type (A-type) and the equilibrium torsional angle in the upper electronic state of this series are quite similar to those of series II. Similarity in the equilibrium torsional angle implies that the torsional potential of the electronic state for series I must be very similar to that of series II, though the Franck−Condon region for the transition must be different. The lower part of the double-minimum potential is generally more harmonic than the upper part, and hence the transitions to the bottom region give an equidistant progression as observed in series I.

Concerning the nature of the electronic state relevant to series I transition, the observed small intensity and the long lifetime suggest that the transition to this electronic state has a forbidden character. That is, the upper electronic state in the zero-order approximation is not accessible from the ground state but actually becomes accessible by coupling with some allowed electronic state. It is important in this respect to remember that the twisted intramolecular charge transfer state in its perpendicular form is not accessible from the ground state because of symmetry. When the torsional angle relaxes from the perpendicular position, the mixing with the LE state becomes feasible and it makes the transition partially allowed. In other words, the vibronic coupling via the torsional vibration makes this state accessible from the ground state. In addition, the new progression (series I) appears only for the NH_2-substituted PA; the NH_2 group has a considerable electron-donating power and makes the electron transfer from the benzene to the anthracene much easier. All these considerations suggest that the upper electronic state for the series I progression is most probably the CT state or at least has significant CT character.

1.3. Possible Interpretation by the Vibrational Coupling. At this point, we consider more closely the possibility that the two progressions may be due to the combination of vibrational modes in the same electronic state. First, it is certain from the reported vibrational analysis of 9-PA that the series II torsional progression is the υ'-progression on the zero-vibrational level of the LE state. Then, if the series I progression originates from the combination of the torsional mode with some other vibration, it is natural to expect series I to appear at shorter wavelengths than series II. However, this is not the case.

Another possibility is special vibrational coupling that significantly changes the Franck−Condon factors for the series I vibronic transition. Let us imagine the two torsional potentials on the different vibrational levels; one is the zero-vibrational level (A) on an upper electronic state and the other is a vibronic level (B) on the same electronic state with a vibrational mode other than the torsion. These two vibrational states may give their own respective torsional progressions. In addition, one can see another torsional progression belonging to B, if the lower torsional levels of B borrow transition intensity from A through some vibrational coupling. This new progression may have equidistant peak spacing because the transition occurs to the lower part of the torsional potential where harmonicity is greater than the upper part. This progression, if it exists, should appear in an energy region similar to the torsional progression of A because the intensity borrowing must be most effective in this region. In our actual observation, however, the transition region of the series I progression is apparently 200 cm^{-1} lower than that of series II. Thus, the possibility of vibrational coupling in the same electronic state should be excluded.

2. Torsional Potentials Belonging to the Two Excited Electronic States. 2.1. Calculations of Torsional Energy Levels and Wave Functions. In general, the torsional motion is assumed to be confined to the single mathematical dimension, and the other degrees of freedom are considered separately. The torsional potential is assumed to have a form of trigonometric series as

$$V(\phi) = \frac{1}{2}\sum_n V_n(1 - \cos n\phi) \tag{1}$$

where ϕ is a torsional angle. The torsional energy level and wave function can be obtained by solving the following wave equation,

$$\left[-\frac{\mathrm{d}}{\mathrm{d}\phi}F(\phi)\frac{\mathrm{d}}{\mathrm{d}\phi} + V(\phi)\right]\psi = E\psi \tag{2}$$

where

$$F(\phi) = \frac{h}{8\pi cI(\phi)} \tag{3}$$

and I is the reduced moment of inertia for the torsional motion. Since the angle dependence of I is very small over the range of ϕ, no significant error is induced by taking F to be constant: 0.2016 cm^{-1} was used for F. The parameters of eq 1, V_n, were determined so as to reproduce the observed peak positions and intensities of the progression. The potential for the series II progression was evaluated by assuming three or four additional lower levels which could not be observed due to unfavorable Franck−Condon factors; the peak assigned at the longest wavelength is not the origin of the series II progression. The inclusion of missing levels is necessary to produce the coupling between the two relevant electronic states. The addition of lower torsional levels has no significant effect on the qualitative shape of the potential except for changing the potential barrier between the double minima. The parameters that were used in the calculations are given in Table 3.

TABLE 3: Parameters (cm^{-1}) for the Ground and Excited State Torsional Potentials of AA and for the Coupling between the LE and CT States

V_n	S_0	LE	CT
V_2	−2653	−2400	−800
V_4	−682	−1680	−1350
V_6	23	−55	300
V_8		10	−85
V_{10}		25	20
V_{12}			−70
V_{14}			−15
ΔE		63	
H_{CL}		42	

2.2. Torsional Potential Belonging to the Ground State. *Symmetry Consideration and the Shape of the Torsional Potential.* For the simulation of the ground state, one can assume the potential curve either with a single minimum or with double minima, as shown in Figure 6. The torsional levels obtained as the solutions of eqs 1 and 2 have their individual symmetric characters, depending on the shape of the potential. When only the even terms are considered in eq 1, the resulting wave function is either symmetric (*s*) or antisymmetric (*a*) with respect to the plane of symmetry at 90°. Each level is doubly degenerate due to the (cosine) symmetry with respect to the plane at 180°. If the torsional potential has a single minimum at 90° (and of course at 270° because of the symmetry), then the even torsional levels are symmetric and odd ones are antisymmetric (case a). For the double-minimum potential (case b), each energy level is quadruply degenerate and contains both *s* and *a* levels. In any case, only $a \leftrightarrow a$ and $s \leftrightarrow s$ transitions are allowed.

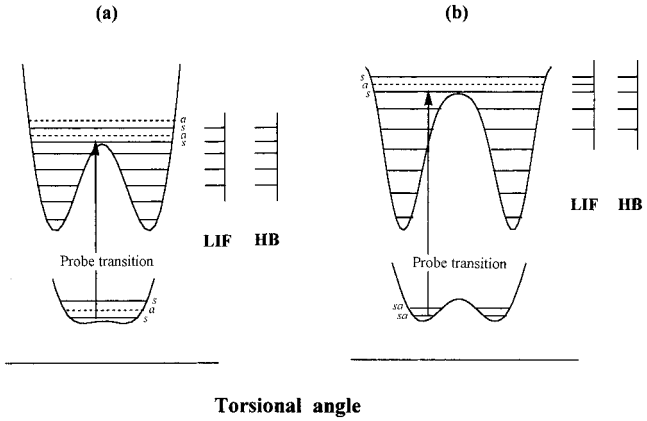

Figure 6. Schematic picture for the LIF and the hole-burning (HB) spectra expected from the selection rule. The two typical cases of the ground state torsional potential function are illustrated: (a) a single-minimum potential and (b) a double-minimum potential.

By combining the above level symmetry and the selection rule with the hole-burning spectroscopy, we can determine the shape of the torsional potential whether it has a single minimum or double minima. In case a, where the lowest torsional level of the ground state is *s*, the vibrational transition occurs only to the symmetric torsional levels of the excited state. Since any transitions observed are $s \Leftrightarrow s$ transitions, the hole-burning spectroscopy using a specific $s \Leftrightarrow s$ transition as a monitor gives the spectrum which completely coincides with the LIF spectrum. Although *s* and *a* levels are split in the region above the potential barrier, we have no means of reaching the *a* levels from the lowest torsional level.

On the other hand, in case b, the lowest torsional level is quadruply degenerate and contains both *s* and *a* levels. All the levels above the barrier are, therefore, accessible from the lowest level. Now, if we set the monitor level in the hole-burning spectroscopy to be a specific *s* level above the barrier, then only *s* levels can give rise to dips in the spectra. Similarly, if an *a* level is used for the monitor, we observe the dip only at *a* levels. Thus the features of the hole-burning spectra depend on the level selected for the monitor, and "missing peaks" are present when compared with the LIF spectra as shown in Figure 6b.

With the above viewpoint in mind, we took the hole-burning spectra for the torsional peaks above the potential barrier. No differences between the LIF and the dip signals were obtained by changing the monitor peak. Therefore, we conclude that the ground state has energy levels with alternating symmetries. Very importantly, this fact means that the equilibrium torsional angle of the ground state is 90°.

So far, many reports have been issued on the peculiar behavior of TICT state formation in ADMA, and some researchers attribute this to the nonperpendicularity of the ground state. Their simple molecular orbital (MO) calculations also showed that the nonperpendicular structure is most stable.[20] Now, the above observation concludes that the equilibrium structure is perpendicular. However, our conclusion does not exclude the possibility of an adiabatic double-minimum potential with a small barrier at 90°. Even though the potential has a double-minimum shape, the lowest energy level could be above the barrier because of the zero-point energy. This is the case for the ground state of AA; the ground state has an adiabatic double-minimum potential with a small barrier of 6.1 cm^{-1}, and hence the lowest level is located above the barrier. In the case of ADMA, as suggested in the previous paper,[14] the 4 cm^{-1} splitting at the bottom level indicates that the barrier is slightly higher than the zero-point energy and gives a tunneling splitting of this amount. In both cases, the essential factor is the flatness of the potential which makes the torsional motion very flexible around 90°.

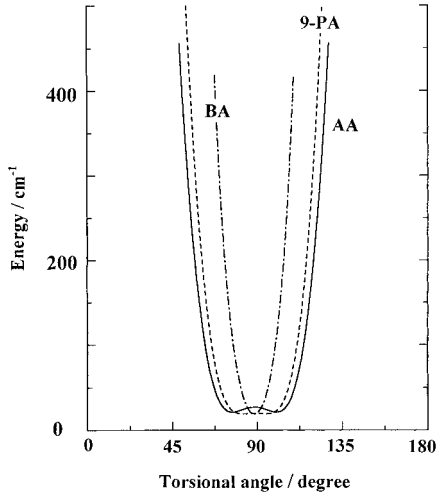

Figure 7. Comparison in the shape of the ground torsional potential among BA, AA, and 9-phenylanthracene (9-PA).

Relation with the Spectral Features Observed in Solution. The broadness of the peak and the tailing toward longer wavelength are the salient features of the absorption spectra of ADMA and also of AA in solution as shown in the preceding paper in this issue. These features are understandable based on the present experiment. That is, the broadness of the peak is a simple reflection of the flatness in the ground state torsional potential. Figure 7 compares the shape of the torsional potential among BA, AA, and 9-phenylanthracene. One may notice that the bulkiness of the rotating moiety is an important factor. The potential of BA is narrow and steep because of the greater bulkiness of anthracene. When the ground state potential is flatter, the Franck−Condon region of the upper electronic state becomes wider in its energy range, which consequently makes the absorption peak broader.

2.3. Torsional Potentials of the Two Electronic States. The potential parameters for the torsional potential of the LE state were determined so that the peak positions and the intensities of the series II progression are reproduced. The parameters are listed in Table 3, and the shape of the potential is given by the solid curve in the upper part of Figure 8. This curve expresses the zero-order potential of the LE state. As a result of coupling with the CT state, the potential as well as the energy levels would be modified. However, we found that the coupling gives only negligible effects on the energy levels and transition intensities of the upper torsional levels in the LE state.

For the CT state, we first roughly estimate the potential parameters from the energy levels of the series I progression. In order to reproduce the peak intensity, we have to consider the coupling between the CT and the LE states, since the series I peaks borrow the intensity from the LE state. The evaluated potential parameters are also listed in Table 3, and the shape of zero-order torsional potential is given in Figure 8 by the dashed line. The detailed procedure for the calculations will be given in the subsequent section.

3. Coupling between the Two Electronic States. 3.1. Method of the Calculations. In order to reproduce the intensity distribution of the series I progression, we consider the coupling between the two electronic states. First, the zero-order torsional levels are calculated for each zero-order electronic state by the

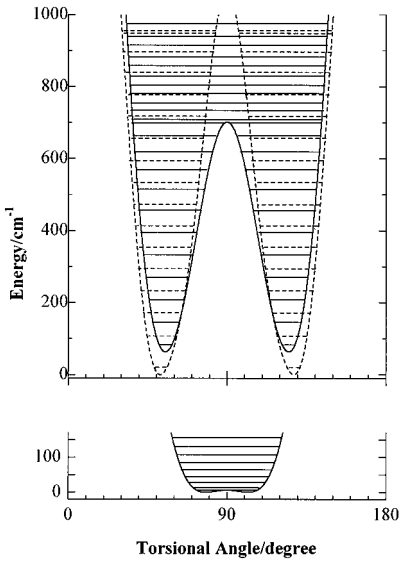

Figure 8. Best-fit ground (lower), the LE (upper, solid line), and the CT (upper, dashed line) state torsional potentials of AA. The two excited state potentials are those of the zero-order electronic states. The energy levels shown in the upper traces are obtained by taking account of the coupling between the zero-order states.

procedure given in section 2.1. The zero-order vibronic wave functions of the LE and the CT states are expressed as

$$|\mathrm{LE}(q,Q)\rangle = |\psi_e^{\mathrm{LE}}(q,Q_0)\psi_{vn}^{\mathrm{LE}}(Q)\rangle$$

$$|\mathrm{CT}(q,Q)\rangle = |\psi_e^{\mathrm{CT}}(q,Q_0)\psi_{vn'}^{\mathrm{CT}}(Q)\rangle$$

where q is the electron coordinate at the equilibrium nuclear configuration Q_0. $\psi_e(q,Q_0)$ is an electronic wave function, and $\psi_{vn}(Q)$ is a vibrational wave function with a vibrational quantum number, n. The coupling Hamiltonian is assumed to have the form $H_{LC}'(\cos 2\phi + 1)$ where H_{LC}' is the electronic coupling term and ϕ is the torsional coordinate; the coupling is zero at 90° and increases with increasing deviation from the perpendicular position. Then, the coupling matrix elements between the zero-order vibronic states can be obtained as

$$\begin{aligned}&\langle\psi_e^{\mathrm{LE}}(q,Q_0)\psi_{vn}^{\mathrm{LE}}(Q)|H_{LC}'(\cos 2\phi+1)|\psi_e^{\mathrm{CT}}(q,Q_0)\psi_{vn'}^{\mathrm{CT}}(Q)\rangle\\ &=\langle\psi_e^{\mathrm{LE}}(q,Q_0)|H_{LC}'|\psi_e^{\mathrm{CT}}(q,Q_0)\rangle\langle\psi_{vn}^{\mathrm{LE}}(Q)|(\cos 2\phi+1)|\psi_{vn'}^{\mathrm{CT}}(Q)\rangle\\ &=H_{LC}\langle\psi_{vn}^{\mathrm{LE}}(Q)|(\cos 2\phi+1)|\psi_{vn'}^{\mathrm{CT}}(Q)\rangle\end{aligned}$$

The matrix elements are calculated using the zero-order wave functions, and the diagonalization of the matrix is performed to obtain the coupled states. Parameters here are H_{LC} and the energy difference between the LE and the CT states, ΔE. The feature of the LIF spectrum was simulated by adjusting these parameters; the energy gap between the two progressions was adjusted by ΔE and the intensity ratio between the progressions was sensitive to the parameter H_{LC}.

3.2. Character of the CT State. The potential curves for the torsional vibration of AA on the two zero-order electronic states are shown in Figure 8, together with the energy levels after the coupling. The fitting parameters for the coupling are also given in Table 3. The result of the simulation is given in Figure 9. The intensities of the corresponding peaks of the LIF spectrum are given by the circles. Note that the simulation does not include the combination bands and hence is much simpler than the observed spectra. The reproducibility of the peak position is quite good for the origin progressions of series I and II, and this fact assures the correctness of the torsional potentials derived.

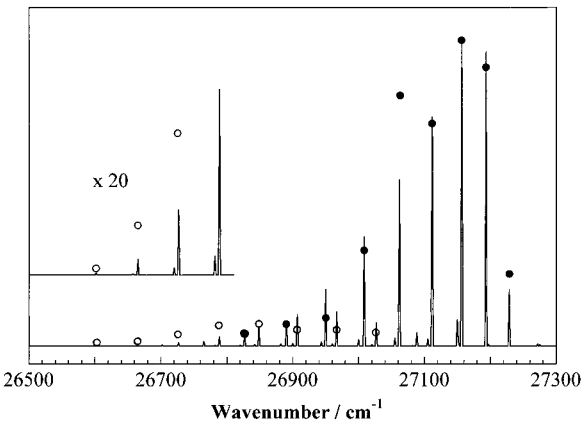

Figure 9. Comparison between the observed and the simulated intensity distributions in the LIF spectra of AA. The simulation includes only the origin progressions of series I (mode A) and II. The circle indicates the intensity of the peak: ○ for series I, ● for series II.

The reproducibility in the transition intensity is also remarkable, again showing the correctness of the assumption. Although the reproducibility in the intensity ratio could be further improved by fine adjustment of the potential parameters, we did not attempt such adjustment in the present study. As described in the previous section, we assume that the intensity of the optical transition to the CT state stems from the oscillator strength of the transition to the LE state. If this is correct, the direction of the transition moment in both progressions (I and II) must be parallel to the anthryl−aniline bond, i.e., an A-type transition. This expectation is in agreement with the observed rotational contours.

The torsional potentials evaluated above indicate that AA is almost halfway to the planar structure in both the LE and the CT electronic states. So far, in many studies, the perpendicular CT state has been implicitly accepted for all TICT molecules, including ADMA.[21] However, such is not necessarily true for the less rigid molecules like AA in less polar environments. The coupling between the CT and the LE states can distort the excited state potential such that the CT state could have minima in a nonperpendicular conformation. The implication of such a nonperpendicular CT state will be discussed later.

3.3. Difference in the Hot Band Intensity between the Two Transitions. At this point, we can provide the explanation for the trend in the hot band intensity discussed in the Results section. For series I peaks all the hot bands are clearly observed, whereas for series II peaks the hot bands gradually disappear with increasing transition energy. Now, the wave function of the zero-vibrational level of the ground state has its maximum amplitude around 90° in the present case. With increasing energy in the ground torsional level (i.e., hot band), the peak of the wave function gradually shifts from 90°, which affects the Franck−Condon overlap with the upper torsional level. That is, the more the upper torsional level deviates from 90°, the more favorable is the Franck−Condon overlap with the hot band level. Since the series II progression is the transition toward the barrier top of the double-minimum potential, the overlap with hot band levels is not favorable. On the other hand, the series I progression corresponds to transitions to the bottom part, which deviates substantially from 90°. Hence, the Franck−Condon overlap is more favorable for hot bands than for the parent band.

4. Interpretation of the Electronic States in Terms of Molecular Orbitals. In order to investigate the nature of the electronically excited states as a function of torsional angle, a

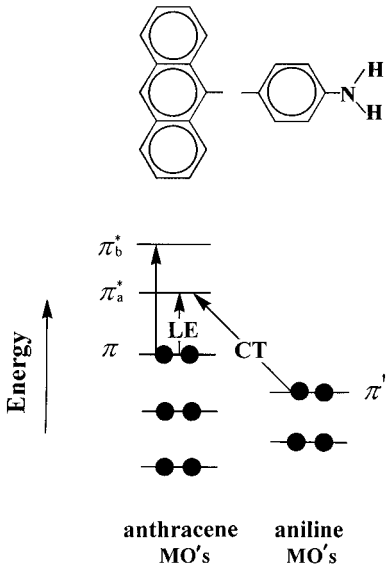

Figure 10. Schematic representation of the molecular orbitals of AA, which is composed of the orbitals either belonging to anthracene or to aniline. The electronic configurations of the two electronically excited states, the LE and the CT states, are depicted.

semiempirical CNDO/S calculation was carried out at several torsional angles. The structure for each moiety was taken from the reported data and assumed to be the same irrespective of the angle. Figure 10 schematically illustrates the relevant molecular orbitals. The lowest LE state (^1L_a) is formed by the promotion of an electron from the π orbital to the vacant π_a* orbital. The second lowest LE state of anthracene (^1L_b) corresponds to the $\pi \rightarrow \pi_b$* transition. The CT formation is not necessarily the electron jump from the lone pair of the N atom to the anthracene but more generally the partial electron transition from the aniline part to the anthracene moiety.

At the perpendicular position, the mixing of the orbitals between the aniline and anthracene parts is quite small. The photoexcitation from the ground state to the CT state is completely forbidden because of symmetry. As the torsional angle relaxes from 90°, the CT state begins to couple with the LE states and the optical transition from the ground state becomes partially allowed. In the perpendicular conformation, the energy level of the CT state is higher than those of the ^1L_a, ^1L_b, and other low-lying LE states. With increasing deviation of the torsional angle from 90°, the mixing of the CT state with the LE states becomes more and more efficient and it lowers the energy levels of the mixed states. Within the framework of the present semiempirical MO calculations we could not achieve the situation where the energy level of the mixed state with high CT character becomes comparable to that of the lowest LE state. However, when the torsional angle is diminished unrealistically to less than 10°, the state with significant CT character can come very close to the lowest one.

5. Implication of the New Electronic State to the Dynamics of CT State Formation. The observation of a new electronic state and the evaluation of its average torsional angle have very important implications for understanding the peculiar behavior of ADMA in the CT state formation. We first discuss the implication of the low-lying CT state (at least the state with strong CT nature) and then describe the meaning of the nonperpendicular CT state in comparison with the CT state formation in BA.

5.1. Implication of the Low-Lying CT State. In the preceding paper in this issue, we discussed the polarity dependence of the fluorescence maximum in terms of a Lippert−Mataga plot. The plot showed that the energy gap between the CT and the LE states in a nonpolar environment is quite small in the case of AA as compared with BA. This is the reason why we can observe the broad CT fluorescence even in a solvent of small polarity, like diethyl ether. In contrast, the fluorescence of BA in diethyl ether mostly comes from the LE state. The low-lying CT state, which is expected from the Lippert−Mataga plot for AA, is actually observed in the present study.

Next, the low-lying CT state is also responsible for the tailing of the absorption spectra observed in the solution phase (preceding paper of this issue). The tailing is observed only for ADMA and AA; the presence of the NH_2 substituent is essential for the low-lying CT state and, therefore, no such tailing is observed for BA and 9-PA. Although the absorption intensity of the series I progression in isolated AA is not very strong, the intensity may be enhanced in the solution phase. Thus, the series I progression shows up as the red tail in the absorption spectrum in solution.

Vibronic coupling between the CT and LE state has been recently proposed in several papers. In the case of 9-(*N*-carbazolyl)anthracene (C9A) observed in a jet, a model of a diabatic surface crossing along the torsional coordinate was suggested for explaining the additional peaks observed.[22] Zachariasse et al.[12] postulated vibronic coupling between the closely-lying LE and the CT states of *N*,*N*-dialkyl-4-aminobenzonitriles in the solution phase. The present experiment offers the first definite example to demonstrate the occurrence of such coupling between the CT and the LE states in a similar energy region.

5.2. Implication of the Nonperpendicular CT State. In many cases, the CT state has been thought to have a single minimum around 90°. In AA, however, the CT state possesses a double-minimum potential with an equilibrium angle of 50°. At this equilibrium angle, it is impossible to have complete charge separation, since the two aromatic moieties interact with each other through conjugation. Therefore, the state possesses only a partial CT character, where the mild charge separation ($\delta^+-\delta^-$) takes place. The present experiment shows that even in an isolated molecule (or in a completely nonpolar environment) the electronic state with some CT character is present close to the LE state.

ADMA is known to be a peculiar molecule whose dynamic behavior in CT state formation is quite complex. Okada et al.[3] suggested from the analysis of the solvent dependence of the transient absorption spectra that intramolecular electron transfer in the excited state of ADMA does not lead to complete charge separation; only a partial CT state is formed. The degree of charge separation depends upon the interaction with polar solvents and also upon the twisting angle between the phenyl and the anthracene rings. It is not possible to explain these results in terms of the simple two-state TICT mechanism which is applicable to BA.

Our findings in the present study provide a clear picture and evidence for the above proposal. The molecules with large flexibility in the torsional motion, like ADMA and AA, can form a partial charge-transfer state as a result of mixing between the LE and CT states. The degree of mixing and hence the charge separation depend on the torsional angle. If the molecule is sitting in a very polar environment, the fully charge-separated state must be significantly stabilized, which favors the perpendicular conformation facilitating full charge transfer. On the other hand, if the environment is less polar, charge separation is not favorable compared with the stabilization by conjugation. Consequently, the equilibrium torsional angle becomes smaller and the electronic state tends to lose the nature of full charge

separation. In this way, the nature of a resulting CT state (the equilibrium structure and the degree of charge separation) is strongly dependent on the solvent polarity. Such a situation makes the behavior of ADMA quite complex and peculiar.

Conclusion

Laser-induced fluorescence excitation spectra of 4-(9-anthryl)-aniline have been observed in a free jet. The LIF spectra are analyzed as composed of two different progressions, both originating from the torsional vibrations around the anthryl−aniline bond. One is the transition common to the phenyl-anthracene derivatives (series II) and the other is a new transition as found only for the NH_2-substituted phenylanthracenes (series I). The hole-burning spectra, hot band analysis, and rotational contour analysis have been carried out to elucidate the origin of the new progression. We conclude that a new low-lying electronic state is responsible for the series I progression. The torsional potential in this new electronic state, as well as those in the ordinary excited and ground states, was evaluated from the observed LIF spectra.

The simulation of the vibrational levels and intensities has also been performed by assuming a coupling between the two electronic states; one is fully allowed and the other is originally forbidden but becomes partially allowed by the coupling through the torsional motion. Such a coupling was confirmed from the fluorescence lifetime measurements. The two electronic states corresponding to series I and II most probably possess the character of CT and LE states, respectively, in the zero-order states. The calculation well reproduced the complex vibrational structure of the observed LIF excitation spectrum.

In an isolated AA molecule, the CT state is found to be nonperpendicular and the charge separation is incomplete. The presence of the NH_2 substituent is responsible for the low-lying CT state while the flexible torsional motion causes the nonperpendicular CT state. These two important findings offer a general picture for multiple CT states, where the polarity of the environment determines the torsional angle and the degree of charge separation as a result of balance between the conjugation and the stabilization of the separated charge by polar solvents. The new electronic state and its torsional potential provide the key to explain the puzzling behavior of ADMA in the CT state formation.

Acknowledgment. The authors thank Prof. Kohei Tamao of the Chemical Research Institute of Kyoto University for his valuable help in synthesizing AA and also Drs. Yo Fujimura and Haruki Ishikawa for their discussions and generous help in carrying out the experiments. The authors are also indebted to Mr. Hiroshi Akagi for his appropriate suggestions and help in doing MO calculations. The authors are obliged to Mr. Koji Arita for his preliminary experiments on the same subject. This work is partially supported by the Grant-in-Aid (numbers 06453022 and 03403002) from the Ministry of Education, Science and Culture. One of the authors (Lee) greatly appreciates the scholarship from the same Ministry.

References and Notes

(1) Werst, D. W.; Brearley, A. M.; Gentry, W. R.; Barbara, P. F. *J. Am. Chem. Soc*. **1987**, *109*, 32.
(2) Mataga, N.; Yao, H.; Okada, T.; Rettig, W. *J. Phys. Chem*. **1989**, *93*, 3383.
(3) Okada, T.; Mataga, N.; Baumann, W.; Siemiarczuk, A. *J. Phys. Chem*. **1987**, *91*, 4490.
(4) Im, H.-S.; Bernstein, E. R. *J. Chem. Phys*. **1988**, *88*, 7337.
(5) Wang, S.; Cai, J.; Sadygov, R.; Lim, E. C. *J. Phys. Chem*. **1995**, *99*, 7416.
(6) August, J.; Palmer, T. F.; Simons, J. P.; Jouvet, C.; Rettig, W. *Chem. Phys. Lett*. **1988**, *145*, 273.
(7) Rettig, W.; Zander, M. *Ber. Bunsen-Ges. Phys. Chem*. **1983**, *87*, 1143.
(8) (a) Schneider, F.; Lippert, E. *Ber. Bunsen-Ges. Phys. Chem*. **1968**, *72*, 1155. (b) Schneider, F.; Lippert, E. *Ber. Bunsen-Ges. Phys. Chem*. **1970**, *74*, 624.
(9) Okada, T.; Fujita, T.; Kubota, M.; Masaki, S.; Mataga, N.; Ide, R.; Sakata, Y.; Misumi, S. *Chem. Phys. Lett*. **1972**, *14*, 563.
(10) (a) Siemiarczuk, A.; Ware, W. R. *J. Phys. Chem*. **1987**, *91*, 3677. (b) Okada, T.; Mataga, N.; Baumann, W.; Siemiarczuk, A. *J. Phys. Chem*. **1987**, *91*, 4490.
(11) Tominaga, K.; Walker, G. C.; Jarzeba, W.; Barbara, P. F. *J. Phys. Chem*. **1991**, *95*, 10475.
(12) Zachariasse, K. A.; Harr, T.; Hebecker, A.; Leinhos, U.; Kuhnle, W. *Pure Appl. Chem*. **1993**, *65*, 1745.
(13) Wortmann, R.; Elich, K.; Lebus, S.; Liptay, W. *J. Chem. Phys*. **1991**, *95*, 6371.
(14) Subaric-Leitis, A.; Monte, Ch.; Roggan, A.; Rettig, W.; Zimmermann, P.; Heinze, J. *J. Chem. Phys*. **1990**, *93*, 4543.
(15) Kajimoto, O.; Hayami, S. *Chem. Phys. Lett*. **1991**, *177*, 219.
(16) Lamdert, W. R.; Felker, P. M.; Syage, J. A.; Zewail, A. H. *J. Chem. Phys*. **1984**, *81*, 2195.
(17) Lee, S.; Arita, K.; Kajimoto, O. *Chem. Phys. Lett*. **1997**, *265*, 579.
(18) (a) Werst, D. W.; Gentry, W. R.; Barbara, P. F. *J. Phys. Chem*. **1985**, *89*, 729. (b) Werst, D. W.; Londo, W. F.; Smith, J. L.; Barbara, P. F. *Chem. Phys. Lett*. **1985**, *118*, 367.
(19) Chernoff, D. A.; Rice, S. A. *J. Chem. Phys*. **1979**, *70*, 2511.
(20) Herbich, J.; Kapturkiewicz, A. *Chem. Phys*. **1993**, *170*, 221.
(21) (a) Grabowski, Z. R.; Rotkiewicz, K.; Siemiarczuk, A.; Cowley, D. J.; Baumann, W. *Nouv. J. Chim*. **1979**, *3*, 443. (b) Rotkiewicz, K.; Grellmann, K. H.; Grabowski, Z. R. *Chem. Phys. Lett*. **1973**, *19*, 315. (c) Grabowski, Z. R.; Rotkiewicz, K.; Siemiarczuk, A. *J. Lumin*. **1979**, *18*, 420.
(22) Monte, Ch.; Roggan, A.; Subraric-Leitis, A.; Rettig, W.; Zimmermann, P. *J. Chem. Phys.* **1993**, *98*, 2580.